

First observation of the decay $\chi_{cJ} \rightarrow \Sigma^+ \bar{p} K_S^0 + c.c. (J = 0, 1, 2)$

M. Ablikim¹, M. N. Achasov^{10,d}, P. Adlarson⁶⁰, S. Ahmed¹⁵, M. Albrecht⁴, M. Alekseev^{59A,59C}, A. Amoroso^{59A,59C}, F. F. An¹, Q. An^{56,44}, Y. Bai⁴³, O. Bakina²⁷, R. Baldini Ferroli^{23A}, I. Balossino^{24A}, Y. Ban^{36,l}, K. Begzsuren²⁵, J. V. Bennett⁵, N. Berger²⁶, M. Bertani^{23A}, D. Bettoni^{24A}, F. Bianchi^{59A,59C}, J. Biernat⁶⁰, J. Bloms⁵³, I. Boyko²⁷, R. A. Briere⁵, H. Cai⁶¹, X. Cai^{1,44}, A. Calcaterra^{23A}, G. F. Cao^{1,48}, N. Cao^{1,48}, S. A. Cetin^{47B}, J. Chai^{59C}, J. F. Chang^{1,44}, W. L. Chang^{1,48}, G. Chelkov^{27,b,c}, D. Y. Chen⁶, G. Chen¹, H. S. Chen^{1,48}, J. Chen¹⁶, M. L. Chen^{1,44}, S. J. Chen³⁴, Y. B. Chen^{1,44}, W. Cheng^{59C}, G. Cibinetto^{24A}, F. Cossio^{59C}, X. F. Cui³⁵, H. L. Dai^{1,44}, J. P. Dai^{39,h}, X. C. Dai^{1,48}, A. Dbeyssi¹⁵, D. Dedovich²⁷, Z. Y. Deng¹, A. Denig²⁶, I. Denysenko²⁷, M. Destefanis^{59A,59C}, F. De Mori^{59A,59C}, Y. Ding³², C. Dong³⁵, J. Dong^{1,44}, L. Y. Dong^{1,48}, M. Y. Dong^{1,44,48}, Z. L. Dou³⁴, S. X. Du⁶⁴, J. Z. Fan⁴⁶, J. Fang^{1,44}, S. S. Fang^{1,48}, Y. Fang¹, R. Farinelli^{24A,24B}, L. Fava^{59B,59C}, F. Feldbauer⁴, G. Felici^{23A}, C. Q. Feng^{56,44}, M. Fritsch⁴, C. D. Fu¹, Y. Fu¹, Q. Gao¹, X. L. Gao^{56,44}, Y. Gao⁵⁷, Y. Gao⁴⁶, Y. G. Gao⁶, B. Garillon²⁶, I. Garzia^{24A}, E. M. Gersabeck⁵¹, A. Gilman⁵², K. Goetzen¹¹, L. Gong³⁵, W. X. Gong^{1,44}, W. Gradl²⁶, M. Greco^{59A,59C}, L. M. Gu³⁴, M. H. Gu^{1,44}, S. Gu², Y. T. Gu¹³, A. Q. Guo²², L. B. Guo³³, R. P. Guo³⁷, Y. P. Guo²⁶, A. Guskov²⁷, S. Han⁶¹, X. Q. Hao¹⁶, F. A. Harris⁴⁹, K. L. He^{1,48}, F. H. Heinsius⁴, T. Held⁴, Y. K. Heng^{1,44,48}, M. Himmelreich^{11,g}, Y. R. Hou⁴⁸, Z. L. Hou¹, H. M. Hu^{1,48}, J. F. Hu^{39,h}, T. Hu^{1,44,48}, Y. Hu¹, G. S. Huang^{56,44}, J. S. Huang¹⁶, X. T. Huang³⁸, X. Z. Huang³⁴, N. Huesken⁵³, T. Hussain⁵⁸, W. Ikegami Andersson⁶⁰, W. Imoehl²², M. Irshad^{56,44}, Q. Ji¹, Q. P. Ji¹⁶, X. B. Ji^{1,48}, X. L. Ji^{1,44}, H. L. Jiang³⁸, X. S. Jiang^{1,44,48}, X. Y. Jiang³⁵, J. B. Jiao³⁸, Z. Jiao¹⁸, D. P. Jin^{1,44,48}, S. Jin³⁴, Y. Jin⁵⁰, T. Johansson⁶⁰, N. Kalantar-Nayestanaki²⁹, X. S. Kang³², R. Kappert²⁹, M. Kavatsyuk²⁹, B. C. Ke¹, I. K. Keshk⁴, A. Khoukaz⁵³, P. Kiese²⁶, R. Kiuchi¹, R. Kliemt¹¹, L. Koch²⁸, O. B. Kolcu^{47B,f}, B. Kopf⁴, M. Kuemmel⁴, M. Kuessner⁴, A. Kupsc⁶⁰, M. Kurth¹, M. G. Kurth^{1,48}, W. Kühn²⁸, J. S. Lange²⁸, P. Larin¹⁵, L. Lavezzi^{59C}, H. Leithoff²⁶, T. Lenz²⁶, C. Li⁶⁰, C. H. Li³¹, Cheng Li^{56,44}, D. M. Li⁶⁴, F. Li^{1,44}, G. Li¹, H. B. Li^{1,48}, H. J. Li^{9,j}, J. C. Li¹, Ke Li¹, L. K. Li¹, Lei Li³, P. L. Li^{56,44}, P. R. Li³⁰, W. D. Li^{1,48}, W. G. Li¹, X. H. Li^{56,44}, X. L. Li³⁸, X. N. Li^{1,44}, Z. B. Li⁴⁵, Z. Y. Li⁴⁵, H. Liang^{1,48}, H. Liang^{56,44}, Y. F. Liang⁴¹, Y. T. Liang²⁸, G. R. Liao¹², L. Z. Liao^{1,48}, J. Libby²¹, C. X. Lin⁴⁵, D. X. Lin¹⁵, Y. J. Lin¹³, B. Liu^{39,h}, B. J. Liu¹, C. X. Liu¹, D. Liu^{56,44}, D. Y. Liu^{39,h}, F. H. Liu⁴⁰, Fang Liu¹, Feng Liu⁶, H. B. Liu¹³, H. M. Liu^{1,48}, Huanhuan Liu¹, Huihui Liu¹⁷, J. B. Liu^{56,44}, J. Y. Liu^{1,48}, K. Liu¹, K. Y. Liu³², Ke Liu⁶, L. Y. Liu¹³, Q. Liu⁴⁸, S. B. Liu^{56,44}, T. Liu^{1,48}, X. Liu³⁰, X. Y. Liu^{1,48}, Y. B. Liu³⁵, Z. A. Liu^{1,44,48}, Zhiqing Liu³⁸, Y. F. Long^{36,l}, X. C. Lou^{1,44,48}, H. J. Lu¹⁸, J. D. Lu^{1,48}, J. G. Lu^{1,44}, Y. Lu¹, Y. P. Lu^{1,44}, C. L. Luo³³, M. X. Luo⁶³, P. W. Luo⁴⁵, T. Luo^{9,j}, X. L. Luo^{1,44}, S. Lusso^{59C}, X. R. Lyu⁴⁸, F. C. Ma³², H. L. Ma¹, L. L. Ma³⁸, M. M. Ma^{1,48}, Q. M. Ma¹, X. N. Ma³⁵, X. X. Ma^{1,48}, X. Y. Ma^{1,44}, Y. M. Ma³⁸, F. E. Maas¹⁵, M. Maggiora^{59A,59C}, S. Maldaner²⁶, S. Malde⁵⁴, Q. A. Malik⁵⁸, A. Mangoni^{23B}, Y. J. Mao^{36,l}, Z. P. Mao¹, S. Marcello^{59A,59C}, Z. X. Meng⁵⁰, J. G. Messchendorp²⁹, G. Mezzadri^{24A}, J. Min^{1,44}, T. J. Min³⁴, R. E. Mitchell²², X. H. Mo^{1,44,48}, Y. J. Mo⁶, C. Morales Morales¹⁵, N. Yu. Muchnoi^{10,d}, H. Muramatsu⁵², A. Mustafa⁴, S. Nakhoul^{11,g}, Y. Nefedov²⁷, F. Nerling^{11,g}, I. B. Nikolaev^{10,d}, Z. Ning^{1,44}, S. Nisar^{8,k}, S. L. Niu^{1,44}, S. L. Olsen⁴⁸, Q. Ouyang^{1,44,48}, S. Pacetti^{23B}, Y. Pan^{56,44}, M. Papenbrock⁶⁰, P. Patteri^{23A}, M. Pelizaeus⁴, H. P. Peng^{56,44}, K. Peters^{11,g}, J. Pettersson⁶⁰, J. L. Ping³³, R. G. Ping^{1,48}, A. Pitka⁴, R. Poling⁵², V. Prasad^{56,44}, M. Qi³⁴, S. Qian^{1,44}, C. F. Qiao⁴⁸, X. P. Qin¹³, X. S. Qin⁴, Z. H. Qin^{1,44}, J. F. Qiu¹, S. Q. Qu³⁵, K. H. Rashid^{58,i}, K. Ravindran²¹, C. F. Redmer²⁶, M. Richter⁴, A. Rivetti^{59C}, V. Rodin²⁹, M. Rolo^{59C}, G. Rong^{1,48}, Ch. Rosner¹⁵, M. Rump⁵³, A. Sarantsev^{27,e}, M. Savrié^{24B}, Y. Schelhaas²⁶, K. Schoenning⁶⁰, W. Shan¹⁹, X. Y. Shan^{56,44}, M. Shao^{56,44}, C. P. Shen², P. X. Shen³⁵, X. Y. Shen^{1,48}, H. Y. Sheng¹, X. Shi^{1,44}, X. D. Shi^{56,44}, J. J. Song³⁸, Q. Q. Song^{56,44}, X. Y. Song¹, S. Sosio^{59A,59C}, C. Sowa⁴, S. Spataro^{59A,59C}, F. F. Sui³⁸, G. X. Sun¹, J. F. Sun¹⁶, L. Sun⁶¹, S. S. Sun^{1,48}, X. H. Sun¹, Y. J. Sun^{56,44}, Y. K. Sun^{56,44}, Y. Z. Sun¹, Z. J. Sun^{1,44}, Z. T. Sun¹, Y. T. Tan^{56,44}, C. J. Tang⁴¹, G. Y. Tang¹, X. Tang¹, V. Thoren⁶⁰, B. Tsednee²⁵, I. Uman^{47D}, B. Wang¹, B. L. Wang⁴⁸, C. W. Wang³⁴, D. Y. Wang^{36,l}, K. Wang^{1,44}, L. L. Wang¹, L. S. Wang¹, M. Wang³⁸, M. Z. Wang^{36,l}, Meng Wang^{1,48}, P. L. Wang¹, R. M. Wang⁶², W. P. Wang^{56,44}, X. Wang^{36,l}, X. F. Wang¹, X. L. Wang^{9,j},

Y. Wang⁴⁵, Y. Wang^{56,44}, Y. F. Wang^{1,44,48}, Y. Q. Wang¹, Z. Wang^{1,44}, Z. G. Wang^{1,44}, Z. Y. Wang¹,
 Z. Y. Wang⁴⁸, Zongyuan Wang^{1,48}, T. Weber⁴, D. H. Wei¹², P. Weidenkaff²⁶, F. Weidner⁵³, H. W. Wen³³,
 S. P. Wen¹, U. Wiedner⁴, G. Wilkinson⁵⁴, M. Wolke⁶⁰, L. H. Wu¹, L. J. Wu^{1,48}, Z. Wu^{1,44}, L. Xia^{56,44},
 Y. Xia²⁰, S. Y. Xiao¹, Y. J. Xiao^{1,48}, Z. J. Xiao³³, Y. G. Xie^{1,44}, Y. H. Xie⁶, T. Y. Xing^{1,48},
 X. A. Xiong^{1,48}, Q. L. Xiu^{1,44}, G. F. Xu¹, J. J. Xu³⁴, L. Xu¹, Q. J. Xu¹⁴, W. Xu^{1,48}, X. P. Xu⁴²,
 F. Yan⁵⁷, L. Yan^{59A,59C}, W. B. Yan^{56,44}, W. C. Yan², Y. H. Yan²⁰, H. J. Yang^{39,h}, H. X. Yang¹,
 L. Yang⁶¹, R. X. Yang^{56,44}, S. L. Yang^{1,48}, Y. H. Yang³⁴, Y. X. Yang¹², Yifan Yang^{1,48}, Z. Q. Yang²⁰,
 M. Ye^{1,44}, M. H. Ye⁷, J. H. Yin¹, Z. Y. You⁴⁵, B. X. Yu^{1,44,48}, C. X. Yu³⁵, J. S. Yu²⁰, T. Yu⁵⁷,
 C. Z. Yuan^{1,48}, X. Q. Yuan^{36,l}, Y. Yuan¹, C. X. Yue³¹, A. Yuncu^{47B,a}, A. A. Zafar⁵⁸, Y. Zeng²⁰,
 B. X. Zhang¹, B. Y. Zhang^{1,44}, C. C. Zhang¹, D. H. Zhang¹, H. H. Zhang⁴⁵, H. Y. Zhang^{1,44}, J. Zhang^{1,48},
 J. L. Zhang⁶², J. Q. Zhang⁴, J. W. Zhang^{1,44,48}, J. Y. Zhang¹, J. Z. Zhang^{1,48}, K. Zhang^{1,48}, L. Zhang¹,
 Lei Zhang³⁴, S. F. Zhang³⁴, T. J. Zhang^{39,h}, X. Y. Zhang³⁸, Y. Zhang^{56,44}, Y. H. Zhang^{1,44},
 Y. T. Zhang^{56,44}, Yang Zhang¹, Yao Zhang¹, Yi Zhang^{9,j}, Yu Zhang⁴⁸, Z. H. Zhang⁶, Z. P. Zhang⁵⁶,
 Z. Y. Zhang⁶¹, G. Zhao¹, J. Zhao³¹, J. W. Zhao^{1,44}, J. Y. Zhao^{1,48}, J. Z. Zhao^{1,44}, Lei Zhao^{56,44},
 Ling Zhao¹, M. G. Zhao³⁵, Q. Zhao¹, S. J. Zhao⁶⁴, T. C. Zhao¹, Y. B. Zhao^{1,44}, Z. G. Zhao^{56,44},
 A. Zhemchugov^{27,b}, B. Zheng⁵⁷, J. P. Zheng^{1,44}, Y. Zheng^{36,l}, Y. H. Zheng⁴⁸, B. Zhong³³,
 L. Zhou^{1,44}, L. P. Zhou^{1,48}, Q. Zhou^{1,48}, X. Zhou⁶¹, X. K. Zhou⁴⁸, X. R. Zhou^{56,44}, Xiaoyu Zhou²⁰,
 Xu Zhou²⁰, A. N. Zhu^{1,48}, J. Zhu³⁵, J. Zhu⁴⁵, K. Zhu¹, K. J. Zhu^{1,44,48}, S. H. Zhu⁵⁵, W. J. Zhu³⁵,
 X. L. Zhu⁴⁶, Y. C. Zhu^{56,44}, Y. S. Zhu^{1,48}, Z. A. Zhu^{1,48}, J. Zhuang^{1,44}, B. S. Zou¹, J. H. Zou¹

(BESIII Collaboration)

¹ *Institute of High Energy Physics, Beijing 100049, People's Republic of China*

² *Beihang University, Beijing 100191, People's Republic of China*

³ *Beijing Institute of Petrochemical Technology, Beijing 102617, People's Republic of China*

⁴ *Bochum Ruhr-University, D-44780 Bochum, Germany*

⁵ *Carnegie Mellon University, Pittsburgh, Pennsylvania 15213, USA*

⁶ *Central China Normal University, Wuhan 430079, People's Republic of China*

⁷ *China Center of Advanced Science and Technology, Beijing 100190, People's Republic of China*

⁸ *COMSATS University Islamabad, Lahore Campus,*

Defence Road, Off Raiwind Road, 54000 Lahore, Pakistan

⁹ *Fudan University, Shanghai 200443, People's Republic of China*

¹⁰ *G.I. Budker Institute of Nuclear Physics SB RAS (BINP), Novosibirsk 630090, Russia*

¹¹ *GSI Helmholtzcentre for Heavy Ion Research GmbH, D-64291 Darmstadt, Germany*

¹² *Guangxi Normal University, Guilin 541004, People's Republic of China*

¹³ *Guangxi University, Nanning 530004, People's Republic of China*

¹⁴ *Hangzhou Normal University, Hangzhou 310036, People's Republic of China*

¹⁵ *Helmholtz Institute Mainz, Johann-Joachim-Becher-Weg 45, D-55099 Mainz, Germany*

¹⁶ *Henan Normal University, Xinxiang 453007, People's Republic of China*

¹⁷ *Henan University of Science and Technology, Luoyang 471003, People's Republic of China*

¹⁸ *Huangshan College, Huangshan 245000, People's Republic of China*

¹⁹ *Hunan Normal University, Changsha 410081, People's Republic of China*

²⁰ *Hunan University, Changsha 410082, People's Republic of China*

²¹ *Indian Institute of Technology Madras, Chennai 600036, India*

²² *Indiana University, Bloomington, Indiana 47405, USA*

²³ *(A)INFN Laboratori Nazionali di Frascati, I-00044, Frascati,*

Italy; (B)INFN and University of Perugia, I-06100, Perugia, Italy

²⁴ *(A)INFN Sezione di Ferrara, I-44122, Ferrara, Italy; (B)University of Ferrara, I-44122, Ferrara, Italy*

²⁵ *Institute of Physics and Technology, Peace Ave. 54B, Ulaanbaatar 13330, Mongolia*

²⁶ *Johannes Gutenberg University of Mainz, Johann-Joachim-Becher-Weg 45, D-55099 Mainz, Germany*

²⁷ *Joint Institute for Nuclear Research, 141980 Dubna, Moscow region, Russia*

- ²⁸ *Justus-Liebig-Universitaet Giessen, II. Physikalisches Institut, Heinrich-Buff-Ring 16, D-35392 Giessen, Germany*
- ²⁹ *KVI-CART, University of Groningen, NL-9747 AA Groningen, The Netherlands*
- ³⁰ *Lanzhou University, Lanzhou 730000, People's Republic of China*
- ³¹ *Liaoning Normal University, Dalian 116029, People's Republic of China*
- ³² *Liaoning University, Shenyang 110036, People's Republic of China*
- ³³ *Nanjing Normal University, Nanjing 210023, People's Republic of China*
- ³⁴ *Nanjing University, Nanjing 210093, People's Republic of China*
- ³⁵ *Nankai University, Tianjin 300071, People's Republic of China*
- ³⁶ *Peking University, Beijing 100871, People's Republic of China*
- ³⁷ *Shandong Normal University, Jinan 250014, People's Republic of China*
- ³⁸ *Shandong University, Jinan 250100, People's Republic of China*
- ³⁹ *Shanghai Jiao Tong University, Shanghai 200240, People's Republic of China*
- ⁴⁰ *Shanxi University, Taiyuan 030006, People's Republic of China*
- ⁴¹ *Sichuan University, Chengdu 610064, People's Republic of China*
- ⁴² *Soochow University, Suzhou 215006, People's Republic of China*
- ⁴³ *Southeast University, Nanjing 211100, People's Republic of China*
- ⁴⁴ *State Key Laboratory of Particle Detection and Electronics, Beijing 100049, Hefei 230026, People's Republic of China*
- ⁴⁵ *Sun Yat-Sen University, Guangzhou 510275, People's Republic of China*
- ⁴⁶ *Tsinghua University, Beijing 100084, People's Republic of China*
- ⁴⁷ *(A)Ankara University, 06100 Tandogan, Ankara, Turkey; (B)Istanbul Bilgi University, 34060 Eyup, Istanbul, Turkey; (C)Uludag University, 16059 Bursa, Turkey; (D)Near East University, Nicosia, North Cyprus, Mersin 10, Turkey*
- ⁴⁸ *University of Chinese Academy of Sciences, Beijing 100049, People's Republic of China*
- ⁴⁹ *University of Hawaii, Honolulu, Hawaii 96822, USA*
- ⁵⁰ *University of Jinan, Jinan 250022, People's Republic of China*
- ⁵¹ *University of Manchester, Oxford Road, Manchester, M13 9PL, United Kingdom*
- ⁵² *University of Minnesota, Minneapolis, Minnesota 55455, USA*
- ⁵³ *University of Muenster, Wilhelm-Klemm-Str. 9, 48149 Muenster, Germany*
- ⁵⁴ *University of Oxford, Keble Rd, Oxford, UK OX13RH*
- ⁵⁵ *University of Science and Technology Liaoning, Anshan 114051, People's Republic of China*
- ⁵⁶ *University of Science and Technology of China, Hefei 230026, People's Republic of China*
- ⁵⁷ *University of South China, Hengyang 421001, People's Republic of China*
- ⁵⁸ *University of the Punjab, Lahore-54590, Pakistan*
- ⁵⁹ *(A)University of Turin, I-10125, Turin, Italy; (B)University of Eastern Piedmont, I-15121, Alessandria, Italy; (C)INFN, I-10125, Turin, Italy*
- ⁶⁰ *Uppsala University, Box 516, SE-75120 Uppsala, Sweden*
- ⁶¹ *Wuhan University, Wuhan 430072, People's Republic of China*
- ⁶² *Xinyang Normal University, Xinyang 464000, People's Republic of China*
- ⁶³ *Zhejiang University, Hangzhou 310027, People's Republic of China*
- ⁶⁴ *Zhengzhou University, Zhengzhou 450001, People's Republic of China*

^a *Also at Bogazici University, 34342 Istanbul, Turkey*

^b *Also at the Moscow Institute of Physics and Technology, Moscow 141700, Russia*

^c *Also at the Functional Electronics Laboratory, Tomsk State University, Tomsk, 634050, Russia*

^d *Also at the Novosibirsk State University, Novosibirsk, 630090, Russia*

^e *Also at the NRC "Kurchatov Institute", PNPI, 188300, Gatchina, Russia*

^f *Also at Istanbul Arel University, 34295 Istanbul, Turkey*

^g *Also at Goethe University Frankfurt, 60323 Frankfurt am Main, Germany*

^h *Also at Key Laboratory for Particle Physics, Astrophysics and Cosmology, Ministry*

of Education; Shanghai Key Laboratory for Particle Physics and Cosmology; Institute of Nuclear and Particle Physics, Shanghai 200240, People's Republic of China

ⁱ Also at Government College Women University, Sialkot - 51310. Punjab, Pakistan.

^j Also at Key Laboratory of Nuclear Physics and Ion-beam Application (MOE) and Institute of Modern Physics, Fudan University, Shanghai 200443, People's Republic of China

^k Also at Harvard University, Department of Physics, Cambridge, MA, 02138, USA

^l Also at State Key Laboratory of Nuclear Physics and Technology, Peking University, Beijing 100871, People's Republic of China

Using E1 radiative transitions $\psi(3686) \rightarrow \gamma\chi_{cJ}$ from a sample of $(448.1 \pm 2.9) \times 10^6$ $\psi(3686)$ events collected with the BESIII detector, the decays $\chi_{cJ} \rightarrow \Sigma^+ \bar{p} K_S^0 + c.c.$ ($J = 0, 1, 2$) are studied. The decay branching fractions are measured to be $\mathcal{B}(\chi_{c0} \rightarrow \Sigma^+ \bar{p} K_S^0 + c.c.) = (3.52 \pm 0.19 \pm 0.21) \times 10^{-4}$, $\mathcal{B}(\chi_{c1} \rightarrow \Sigma^+ \bar{p} K_S^0 + c.c.) = (1.53 \pm 0.10 \pm 0.08) \times 10^{-4}$, and $\mathcal{B}(\chi_{c2} \rightarrow \Sigma^+ \bar{p} K_S^0 + c.c.) = (8.25 \pm 0.83 \pm 0.49) \times 10^{-5}$, where the first and second uncertainties are the statistical and systematic ones, respectively. No evident intermediate resonances are observed in the studied processes.

PACS numbers: 13.25.Gv, 14.40.Be, 12.38.Qk, 11.30.Er

I. INTRODUCTION

The first charmonium states with $J^{PC} = J^{++}$ discovered after the J/ψ and $\psi(3686)$ were the χ_{cJ} ($J = 0, 1, 2$) particles. Quarkonium systems, especially charm anti-charm states, are regarded as a unique laboratory to study the interplay between perturbative and nonperturbative effects in quantum chromodynamics (QCD). Experimental studies of charmonium decays can test QCD and QCD-based effective field theory calculations. The χ_{cJ} states belong to the charmonium P -wave spin triplet, and therefore cannot be produced via a single virtual-photon exchange in electron-positron annihilations as are the J/ψ and $\psi(3686)$. Until now the understanding of these states has been limited by the availability of experimental data. The world's largest data set of $\psi(3686)$ events [1] collected with the BESIII [2] detector, provides a unique opportunity for detailed studies of χ_{cJ} decays, since they are copiously produced in $\psi(3686)$ radiative transitions with branching fractions of about 9% each [3].

Many excited baryon states have been discovered by BaBar, Belle, CLEO, BESIII, and other experiments in the past decades [3], but the overall picture of these states is still unclear. While many predicted states have not yet been observed, many states that do not agree with quark model predictions are observed (for a review see Ref. [4]). Therefore the search for new excited baryon states is important to improve knowledge of the baryon spectrum and the understanding of the underlying processes which describe confinement in the nonperturbative QCD regime. Experimentally, exclusive decays of χ_{cJ} to baryon anti-baryon ($B\bar{B}$) pairs, such as $p\bar{p}$, $\Sigma\bar{\Sigma}$, $\Lambda\bar{\Lambda}$ [5–8], have been investigated. How-

ever, there are only a few experimental studies of χ_{cJ} to $B\bar{B}M$ (M stands for meson). These channels are ideal to search for new excited baryons in intermediate states, which decay into $\bar{B}M$ and BM .

This paper reports the first measurements of the branching fractions of $\chi_{cJ} \rightarrow \Sigma^+ \bar{p} K_S^0 + c.c.$ via the radiative transition $\psi(3686) \rightarrow \gamma\chi_{cJ}$, where $\Sigma^+ \rightarrow p\pi^0$, $K_S^0 \rightarrow \pi^+\pi^-$, and $\pi^0 \rightarrow \gamma\gamma$. The charge-conjugate state ($c.c.$) is included unless otherwise stated. We also report on a search for possible excited baryon states in the invariant-mass spectra of $\bar{p}K_S^0$, and $\Sigma^+ K_S^0$.

II. BESIII DETECTOR

The BESIII detector is a magnetic spectrometer located at the Beijing Electron Positron Collider (BEPCII) [9]. The cylindrical core of the BESIII detector consists of a helium-based multilayer drift chamber (MDC), a plastic scintillator time-of-flight system (TOF), and a CsI (Tl) electromagnetic calorimeter (EMC), which are all enclosed in a superconducting solenoidal magnet providing a 1.0 T magnetic field. The solenoid is supported by an octagonal flux-return yoke with resistive plate counter muon identifier modules interleaved with steel. The acceptance of charged particles and photons is 93% over 4π solid angle. The charged-particle momentum resolution at 1 GeV is 0.5%, and the dE/dx resolution is 6% for the electrons from Bhabha scattering at 1 GeV. The EMC measures photon energies with a resolution of 2.5% (5%) at 1 GeV in the barrel (end-cap) region. The time resolution of the TOF barrel part is 68 ps, while that of the end-cap part is 110 ps.

III. DATA SET AND MONTE CARLO SIMULATION

This analysis is based on a sample of $(448.1 \pm 2.9) \times 10^6$ $\psi(3686)$ events [1] collected with the BESIII detector.

GEANT4-based [10] Monte Carlo (MC) simulation data are used to determine detector efficiency, optimize event selection, and estimate background contributions. Inclusive MC samples were produced to determine contributions from dominant background channels. The production of the initial $\psi(3686)$ resonance is simulated by the MC event generator KKMC [11, 12], and the known decay modes are modeled with EVTGEN [13, 14] using the branching fractions summarized and averaged by the Particle Data Group (PDG) [3], while the remaining unknown decays are generated by LUNDCHARM [15]. The final states are propagated through the detector system using GEANT4 software.

In addition, for the optimization of the selection criteria and the determination of the efficiency, exclusive MC data sets with 4×10^5 events are generated for each signal mode. Here, the $\psi(3686) \rightarrow \gamma\chi_{cJ}$ decay is generated assuming an E1 transition [16, 17], where the photon polar angle θ in the e^+e^- center-of-mass frame is distributed according to $(1 + \lambda \cos^2 \theta)$. For $J = 0, 1$, and 2 , λ is set to $1, -\frac{1}{3}$, and $\frac{1}{13}$, respectively. The decays $\chi_{cJ} \rightarrow \Sigma^+ \bar{p} K_S^0, \Sigma^+ \rightarrow p \pi^0, K_S^0 \rightarrow \pi^+ \pi^-, \pi^0 \rightarrow \gamma\gamma$ are generated by using the phase-space model (PHSP).

IV. DATA ANALYSIS

For the reaction channel $\psi(3686) \rightarrow \gamma\chi_{cJ}$, with $\chi_{cJ} \rightarrow \Sigma^+ \bar{p} K_S^0, \Sigma^+ \rightarrow p \pi^0, \pi^0 \rightarrow \gamma\gamma$, and $K_S^0 \rightarrow \pi^+ \pi^-$, the final-state particles are $p\bar{p}\pi^+\pi^-\gamma\gamma\gamma$. Charged tracks must be in the active region of the MDC, corresponding to $|\cos \theta| < 0.93$, where θ is the polar angle of the charged track with respect to the beam direction. For the anti-proton (\bar{p}), the point of closest approach to the interaction point (IP) must be within ± 1 cm in the plane perpendicular to the beam (R_{xy}) and ± 10 cm along the beam direction (V_z). Due to the long lifetime of the K_S^0 and Σ^+ , there is no requirement on R_{xy} or V_z for the track candidates used to form the K_S^0 or Σ^+ candidates. Photon candidates are reconstructed by summing the energy deposition in the EMC crystals produced by the electromagnetic showers. The minimum energy necessary for counting a photon as a photon candidate is 25 MeV for barrel showers ($|\cos \theta| < 0.8$) and 50 MeV for end-cap showers

($0.86 < |\cos \theta| < 0.92$). To eliminate showers originating from charged particles, a photon cluster must be separated by at least 10° from any charged track. The timing of the shower is required to be within 700 ns from the reconstructed event start time to suppress noise and energy deposits unrelated to the event. Events with two positively charged tracks, two negatively charged tracks, and at least three good photons are selected for further analysis. The TOF (both end-cap and barrel) and dE/dx measurements for each charged track are used to calculate the p-value based on the χ_{PID}^2 values for the hypotheses that a track is a pion, kaon, or proton. Two oppositely charged tracks are identified as a proton/anti-proton pair if their proton hypothesis p-values are greater than their kaon or pion hypothesis p-values. The remaining charged tracks are considered as pions by default. The numbers of protons and anti-protons as well as the negatively and positively charged pions should be equal to one.

The K_S^0 candidate is reconstructed with a pair of oppositely charged pions. To suppress events from combinatorial background contributions, we require that the $\pi^+\pi^-$ pair is produced at a common vertex [18].

Next a four-constraint (4C) kinematic fit imposing energy-momentum conservation is performed under the $p\bar{p}\pi^+\pi^-\gamma\gamma\gamma$ hypothesis. If there are more than three photon candidates in an event, the combination with the smallest χ_{4C}^2 is retained, and its χ_{4C}^2 is required to be less than those for the $p\bar{p}\pi^+\pi^-\gamma\gamma$ and $p\bar{p}\pi^+\pi^-\gamma\gamma\gamma\gamma$ hypotheses. The value of χ_{4C}^2 is required to be less than 50. For the selected signal candidates, the $\gamma\gamma$ combination ($\gamma_1\gamma_2$) with an invariant mass closest to the π^0 mass is reconstructed as π^0 candidate, and the remaining one (γ_3) is considered to be the radiative photon from the $\psi(3686)$ decay. The $\gamma\gamma$ invariant mass is required to satisfy $|M_{\gamma\gamma} - m_{\pi^0}| < 15 \text{ MeV}/c^2$. Here and throughout the text, M_i represents a measured invariant mass and m_i represents the nominal mass of the particle(s) i [3]. To reduce background events with $\bar{\Lambda} \rightarrow \bar{p}\pi^+$, $|M_{\bar{p}\pi^+} - m_{\Lambda}| > 6 \text{ MeV}/c^2$ is required. Figure 1 shows the scatter plot of the $\pi^+\pi^-$ invariant mass versus the $p\pi^0$ invariant mass of data. To select events which contain both a K_S^0 and a Σ^+ candidate, $|M_{\pi^+\pi^-} - m_{K_S^0}| < 8 \text{ MeV}/c^2$ and $|M_{p\pi^0} - m_{\Sigma^+}| < 20 \text{ MeV}/c^2$ are required (black solid box in Fig. 1). The widths of the mass intervals are chosen to be 3 times the invariant-mass resolution.

The $\Sigma^+ \bar{p} K_S^0$ invariant-mass distributions of the 937 events that passed all selection criteria and the MC simulated events are shown in Fig. 2. Clear signals are observed in the χ_{c0} , χ_{c1} , and χ_{c2} mass

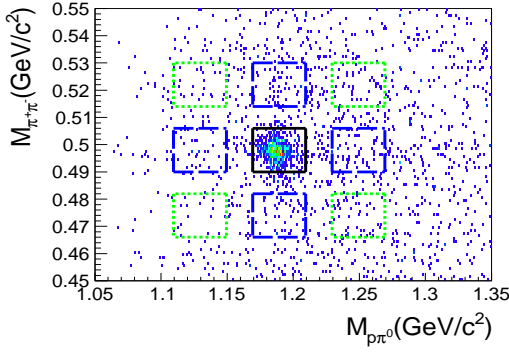


Figure 1. The distribution of the $\pi^+\pi^-$ invariant mass versus the $p\pi^0$ invariant mass. The black solid box in the center is the signal region, the blue long dashed boxes show the K_S^0 and Σ^+ mass sideband regions, and the green dashed boxes are the events from non- K_S^0 and non- Σ^+ candidates.

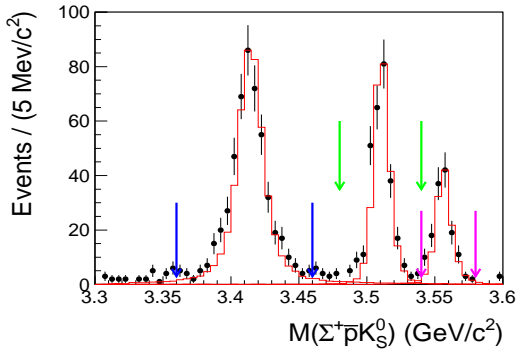


Figure 2. The $\Sigma^+ \bar{p}K_S^0$ invariant-mass distribution in the vicinity of the χ_{cJ} states. Dots with error bars are data, the red solid line histogram is the χ_{cJ} line shape from the MC simulation, and the arrows indicate the χ_{c0} , χ_{c1} , and χ_{c2} signal regions.

regions. The χ_{c0} , χ_{c1} , and χ_{c2} decays are defined as [3.36, 3.46], [3.48, 3.54], and [3.54, 3.58] GeV/c^2 , respectively, as indicated with arrows in Fig. 2.

A hint of a structure in the invariant-mass distribution of the $\bar{p}K_S^0$ subsystem in the χ_{c0} signal region can be seen in Fig. 3(a). Considering the width and mass, it is most likely the $\bar{\Sigma}(1940)^-$ with $M = 1940 \text{ MeV}/c^2$, $\Gamma = 220 \text{ MeV}$, and $I(J^P) = 1(\frac{3}{2}^-)$ [3]. Other excited Σ^* states are most likely excluded because their widths are much larger. For the fit to the invariant-mass distribution $M_{\bar{p}K_S^0}$, several contributions are considered, namely the line shape from the phase-space model, the normalized K_S^0 and Σ^+ mass sidebands in the χ_{c0} signal region (described in detail in the background analysis), and the $\bar{\Sigma}(1940)^-$

signal from the MC simulation, where the mass and width of $\bar{\Sigma}(1940)^-$ are fixed to the world average values [3]. To estimate the statistical signal significance of the $\bar{\Sigma}(1940)^-$ contribution, we use the quantity $\sqrt{-2 \ln(\mathcal{L}_0/\mathcal{L}_{\text{max}})}$, where \mathcal{L}_0 and \mathcal{L}_{max} are the likelihoods of the fits without and with $\bar{\Sigma}(1940)^-$ signal, respectively. The statistical significance of the $\bar{\Sigma}(1940)^-$ signal is obtained to be 3.2σ . The signal significance is reduced to 2.3σ if the width of $\bar{\Sigma}(1940)^-$ is taken as the lower value of 150 MeV [3]. For all other invariant-mass distributions of the two-body subsystems, the description using the phase-space model is in good agreement with data. For example, the $\bar{p}K_S^0$ mass distributions from data and MC simulations in the χ_{c1} and χ_{c2} signal regions are shown in Figs. 3(b) and 3(c).

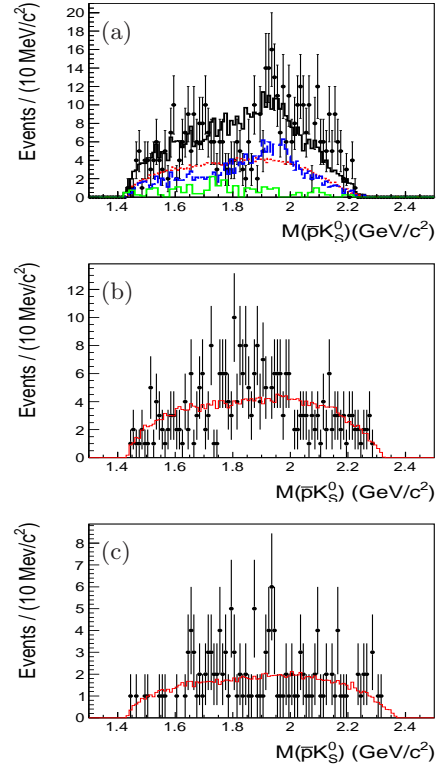


Figure 3. The $\bar{p}K_S^0$ invariant-mass distributions in the (a) χ_{c0} , (b) χ_{c1} , and (c) χ_{c2} signal regions. The dots with error bars are data, the red lines are the contributions from the corresponding MC simulations based on the phase-space model. For plot (a), the black solid line is the fit result, the blue long-dashed curve is the contribution from $\chi_{c0} \rightarrow \Sigma^+ \bar{\Sigma}(1940)^-$, and the green solid line is the contribution from the normalized K_S^0 and Σ^+ mass sideband regions.

Possible background contributions are studied

with the inclusive MC sample of 5.06×10^8 simulated $\psi(3686)$ decays. Peaking background contributions in the χ_{cJ} mass regions are dominated by the channels $\chi_{cJ} \rightarrow \bar{\Delta}^- \pi^+ \Delta^0 (\bar{\Delta}^- \rightarrow \bar{p} \pi^0, \Delta^0 \rightarrow p \pi^-)$ and $\chi_{cJ} \rightarrow p \bar{p} \rho^+ \pi^- (\rho^+ \rightarrow \pi^+ \pi^0)$. Other background events, mainly from the channels $\psi(3686) \rightarrow \Sigma^+ \bar{p} K^* (\Sigma^+ \rightarrow p \pi^0, K^* \rightarrow K_S^0 \pi^0, K_S^0 \rightarrow \pi^+ \pi^-)$, $\psi(3686) \rightarrow K_S^0 \bar{\Delta}^- \Sigma^+ (\bar{\Delta}^- \rightarrow \bar{p} \pi^0, \Sigma^+ \rightarrow p \pi^0, K_S^0 \rightarrow \pi^+ \pi^-)$ and $\psi(3686) \rightarrow J/\psi \pi^0 \pi^0 (J/\psi \rightarrow p \bar{\Delta}^0 \pi^-, \bar{\Delta}^0 \rightarrow \bar{p} \pi^+)$ are not peaking in the χ_{cJ} mass regions. The amount of background events is estimated by using the normalized K_S^0 and Σ^+ mass sideband events, as shown in Fig. 1. The blue long dashed boxes are the selected K_S^0 mass sidebands ($1.1694 < M_{p\pi^0} < 1.2094$ GeV/ c^2 , $0.466 < M_{\pi^+\pi^-} < 0.482$ GeV/ c^2 and $0.514 < M_{\pi^+\pi^-} < 0.530$ GeV/ c^2) and the Σ^+ mass sidebands ($0.49 < M_{K_S^0} < 0.506$ GeV/ c^2 , $1.1094 < M_{p\pi^0} < 1.1494$ GeV/ c^2 and $1.2294 < M_{p\pi^0} < 1.2694$ GeV/ c^2), and the green dashed boxes are those from non- K_S^0 and non- Σ^+ sidebands ($1.1094 < M_{p\pi^0} < 1.1494$ GeV/ c^2 and $1.2294 < M_{p\pi^0} < 1.2694$ GeV/ c^2 , $0.466 < M_{\pi^+\pi^-} < 0.482$ GeV/ c^2 and $0.514 < M_{\pi^+\pi^-} < 0.530$ GeV/ c^2). The normalized background contribution in the χ_{cJ} mass regions is estimated as half of the total number of events in the four blue sideband regions minus one quarter of the total number of events in the four green sideband regions of Fig. 1, and shown as a green-shaded histogram in Fig. 4.

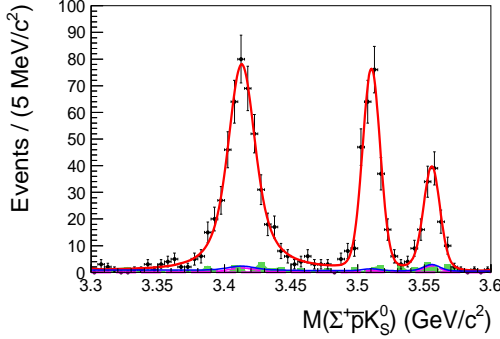


Figure 4. Fit to the $\Sigma^+ \bar{p} K_S^0$ invariant-mass distribution in the χ_{cJ} mass region of $[3.3, 3.6]$ GeV/ c^2 . Dots with error bars are data, the red solid curve shows the result of the unbinned maximum-likelihood fit, the green-shaded histograms are the events from the normalized K_S^0 and Σ^+ mass sidebands, the blue solid line is sum of the peaking and flat background components, and the violet long dashed curve is the contribution of the peaking background normalized according to the sideband events.

An unbinned maximum-likelihood fit to the $\Sigma^+ \bar{p} K_S^0$ invariant-mass distribution is performed

for the total selected signal candidates, as shown in Fig. 4. The complete formula for the fit is $PDF_{\text{total}} = N_1 \times PDF_{\text{signal}} + N_2 \times PDF_{\text{peakingbkg}} + N_3 \times PDF_{\text{flatbkg}}$. The parameters N_1 and N_3 are free, and N_2 is fixed to the number of the events determined from the K_S^0 and Σ^+ mass sidebands.

Here, PDF_{signal} is the sum of the signal line shapes of the three χ_{cJ} resonances each convolved with a Gaussian function related to the χ_{cJ} mass resolution, where the width of the Gaussian function is fixed to each of the MC simulated value. The line shape of each resonance is described by:

$$PDF_{\text{signal}, \chi_{cJ}} = BW(M) \times E_\gamma^3 \times D(E_\gamma), \quad (1)$$

where M is the $\Sigma^+ \bar{p} K_S^0$ invariant mass, $BW(M) = \frac{1}{(M - m_{\chi_{cJ}})^2 + 0.25 \Gamma_{\chi_{cJ}}^2}$ is the Breit-Wigner function, with $m_{\chi_{cJ}}$ and $\Gamma_{\chi_{cJ}}$ the mass and width of the corresponding χ_{cJ} , $E_\gamma = \frac{m_{\psi(3686)}^2 - M^2}{2m_{\psi(3686)}}$ is the energy of the transition photon in the rest frame of $\psi(3686)$ and $D(E_\gamma)$ is the damping factor which suppresses the divergent tail due to the E_γ^3 dependence of PDF_{signal} . It is described by $\exp(-E_\gamma^2/8\beta^2)$ where β is one of the free parameters in the fit. For all three resonances the same β value is required. The fit result $\beta = (68.7 \pm 13.0)$ MeV is consistent with the value measured by the CLEO experiment [19].

The peaking background component $PDF_{\text{peakingbkg}}$ is the same as the signal distribution. It is used to describe the distribution of the normalized events from the K_S^0 and Σ^+ mass sidebands where clearly the three χ_{cJ} resonances can be identified. The PDF_{flatbkg} is described by a first-order polynomial.

For the unbinned maximum-likelihood fit, β , the masses and widths of the χ_{cJ} resonances, and the two coefficients of the polynomial are taken as free parameters. The event yields of the fitted $\chi_{cJ} \rightarrow \Sigma^+ \bar{p} K_S^0$ signals are listed in Table I.

The branching fractions for $\chi_{cJ} \rightarrow \Sigma^+ \bar{p} K_S^0$ are calculated by

$$\mathcal{B}(\chi_{cJ} \rightarrow \Sigma^+ \bar{p} K_S^0) = \frac{N_{\text{obs}}^{\chi_{cJ}}}{N_{\psi(3686)} \times \epsilon \times \prod_j \mathcal{B}_j}, \quad (2)$$

where $N_{\psi(3686)}$ is the total number of $\psi(3686)$ events, ϵ is the corresponding detection efficiency as listed in Table I, which is obtained by weighting the simulated Dalitz plot distribution with the distribution from data, and $\prod_j \mathcal{B}_j = \mathcal{B}(\psi(3686) \rightarrow \gamma \chi_{cJ}) \times \mathcal{B}(\Sigma^+ \rightarrow p \pi^0) \times \mathcal{B}(K_S^0 \rightarrow \pi^+ \pi^-) \times \mathcal{B}(\pi^0 \rightarrow \gamma \gamma)$, where the branching fractions are taken from the PDG [3]. The results of the branching-fraction calculation for the decays $\chi_{cJ} \rightarrow \Sigma^+ \bar{p} K_S^0$ are also listed

Table I. Number of signal events ($N_{\text{obs}}^{\chi_{cJ}}$), detection efficiency (ϵ), and branching fractions $\mathcal{B}(\chi_{cJ} \rightarrow \Sigma^+ \bar{p} K_S^0)$, where the first uncertainty is statistical and the second is systematic.

Mode	$N_{\text{obs}}^{\chi_{cJ}}$	$\epsilon(\%)$	$\mathcal{B}(\chi_{cJ} \rightarrow \Sigma^+ \bar{p} K_S^0)$
$\chi_{c0} \rightarrow \Sigma^+ \bar{p} K_S^0$	493 ± 26	9.05 ± 0.05	$(3.52 \pm 0.19 \pm 0.21) \times 10^{-4}$
$\chi_{c1} \rightarrow \Sigma^+ \bar{p} K_S^0$	258 ± 17	10.96 ± 0.05	$(1.53 \pm 0.10 \pm 0.08) \times 10^{-4}$
$\chi_{c2} \rightarrow \Sigma^+ \bar{p} K_S^0$	129 ± 13	10.40 ± 0.05	$(8.25 \pm 0.83 \pm 0.49) \times 10^{-5}$

in Table I with statistical and systematic uncertainties.

V. SYSTEMATIC UNCERTAINTIES

The systematic uncertainties on the $\chi_{cJ} \rightarrow \Sigma^+ \bar{p} K_S^0$ branching-fraction measurements are listed in Table II.

The systematic uncertainty of the photon-detection efficiency is studied by considering the decay $J/\psi \rightarrow \pi^+ \pi^- \pi^0$ [20] and is about 1% for each photon, so 3% is assigned for the three photons in the final states.

The uncertainty related to the particle identification (PID) and tracking of the proton and anti-proton is studied with the control samples of J/ψ and $\psi(3686) \rightarrow p \bar{p} \pi^+ \pi^-$ [21]. The average differences of efficiencies between MC simulations and data are 0.4%, 0.4%, and 0.3% for the proton from χ_{c0} , χ_{c1} , and χ_{c2} decays, respectively, with the transverse momentum and angle region of our signal channel considered. Similarly for \bar{p} , they are 0.4%, 0.3%, and 0.3%, respectively, so the uncertainties on the proton and anti-proton pair PID and tracking are 0.6%, 0.5%, and 0.4% for χ_{c0} , χ_{c1} , and χ_{c2} decays, respectively.

The uncertainty associated with the 4C kinematic fit comes from the inconsistency between data and MC simulation, as described in detail in Ref. [22]. In this analysis, we take the efficiency with the correction as the nominal value, and the differences between the efficiencies with and without correction, 0.4%, 0.4%, and 0.3% for χ_{c0} , χ_{c1} , and χ_{c2} , respectively, as the systematic uncertainties from the kinematic fit.

The uncertainty associated with the K_S^0 reconstruction is studied using $J/\psi \rightarrow K^*(892)^\pm K^\mp$, $K^*(892)^\pm \rightarrow K_S^0 \pi^\pm$ and $J/\psi \rightarrow \phi K_S^0 K^\pm \pi^\mp$ control samples and is estimated to be 1.2% [23].

The uncertainty related with the π^0 (K_S^0 , Σ^+) mass window requirement is studied by fitting the π^0 (K_S^0 , Σ^+) mass distributions of data and signal MC simulation with a free Crystal Ball (Gaussian, Gaussian) function and a first-order Chebyshev polynomial function. We obtained the selection efficiency

of the π^0 (K_S^0 , Σ^+) mass region, which is the ratio of the numbers of π^0 (K_S^0 , Σ^+) events with and without the π^0 (K_S^0 , Σ^+) mass window, determined by integrating the fitted signal shape. The difference in efficiency between data and MC simulation, 0.3% (0.3%, 0.1%), is assigned as the systematic uncertainty. The systematic uncertainty from the veto of the Λ mass window is negligible due to the high detection efficiency.

The uncertainty of the detection efficiency is studied by changing the number of bins in the Dalitz plot. The maximum differences of the signal detection efficiency, 1.0%, 0.5% and 0.4%, are taken as uncertainties for χ_{c0} , χ_{c1} , and χ_{c2} decays, respectively. The uncertainty of assuming $\psi(3686) \rightarrow \gamma \chi_{c1}(\chi_{c2})$ as pure E1 transition is studied by considering the contribution from higher order multiple amplitudes [24] in the MC simulation, the differences of the efficiency, 0.8% for χ_{c1} and 0.2% for χ_{c2} , are taken as the systematic uncertainties. For $\chi_{c0} \rightarrow \Sigma^+ \bar{p} K_S^0$, there is a possible structure in the $\bar{p} K_S^0$ invariant distribution. The corresponding systematic uncertainty is estimated by mixing $\chi_{c0} \rightarrow \Sigma^+ \bar{\Sigma}(1940)^-$ MC sample and the PHSP signal MC sample in a proportion, which is obtained from fitting $M_{\bar{p} K_S^0}$ distribution. The difference between the efficiencies before and after mixing, 0.1%, is considered to be the systematic uncertainty. The total uncertainties associated with the efficiency for χ_{c0} , χ_{c1} , and χ_{c2} are 1.0%, 0.9%, and 0.4%, respectively.

The systematic uncertainty due to the signal line shape is considered by changing the damping factor from $\exp(-E_\gamma^2/8\beta^2)$ to $\frac{E_0^2}{E_0 E_\gamma + (E_0 - E_\gamma)^2}$ used by KEDR [25], where $E_0 = \frac{m_{\psi(3686)}^2 - m_{\chi_{cJ}}^2}{2m_{\psi(3686)}}$ is the peak energy of the transition photon, the differences in the fit results for χ_{c0} , χ_{c1} , and χ_{c2} , 1.4%, 1.9%, and 0.4% are assigned as the systematic uncertainties.

The uncertainty associated with the detector resolution is studied by making the width of the Gaussian function to be free, no changes are found for the χ_{c0} , χ_{c1} , and χ_{c2} signal yields, thus these uncertainties are neglected.

The systematic uncertainties due to the χ_{c0} , χ_{c1} , and χ_{c2} mass and width in the fit are studied by

changing them from free to the world average values [3]. The differences of the χ_{c0} , χ_{c1} , and χ_{c2} signal yields, 3.0%, 0.4% and 3.9% are taken as the systematic uncertainties.

The uncertainty from the determination of χ_{cJ} signal events due to the fit range is obtained from the maximum difference in the fit results by changing the fit range from [3.30, 3.60] GeV/ c^2 to [3.30, 3.65] GeV/ c^2 or [3.25, 3.60] GeV/ c^2 . The maximum differences in the fitted yields for χ_{c0} , χ_{c1} , and χ_{c2} are 0.9%, 1.4%, and 0.8%, respectively.

The uncertainty due to the estimation of the background contribution using the K_S^0 and Σ^+ mass sidebands can be estimated by changing the sideband ranges. Changing the mass range of K_S^0 from [0.466, 0.482], [0.514, 0.530] GeV/ c^2 to [0.464, 0.480], [0.516, 0.532] GeV/ c^2 , and the mass range of Σ^+ from [1.1094, 1.1494], [1.2294, 1.2694] GeV/ c^2 to [1.1074, 1.1474], [1.2314, 1.2714] GeV/ c^2 , and varying the non- K_S^0 , non- Σ^+ mass region accordingly, the differences of χ_{c0} , χ_{c1} , and χ_{c2} signal yields are 0.3%, 0.1%, and 0.5%, respectively. The uncertainty from the shape of the non- χ_{cJ} background is estimated by changing the polynomial degree from the first to the second in fitting the $\Sigma^+ \bar{p} K_S^0$ invariant mass, and the differences in the fit results are 2.8%, 1.4%, and 1.4%, respectively. The total uncertainties associated with the background shape are 2.8%, 1.4%, and 1.5% for χ_{c0} , χ_{c1} , and χ_{c2} decays, respectively.

The systematic uncertainties due to the secondary branching fractions of $\psi(3686) \rightarrow \gamma \chi_{c0}$ (χ_{c1} , χ_{c2}), $\Sigma^+ \rightarrow p \pi^0$, $K_S^0 \rightarrow \pi^+ \pi^-$, and $\pi^0 \rightarrow \gamma \gamma$ are 2.0% (2.5%, 2.1%), 0.6%, 0.07%, and 0.03% [3] respectively. Therefore, the uncertainties of the secondary branching fractions are 2.1%, 2.6% and 2.2% for χ_{c0} , χ_{c1} , and χ_{c2} decays, respectively.

The number of $\psi(3686)$ events is determined to be $(448.1 \pm 2.9) \times 10^6$ by counting inclusive hadronic events from $\psi(3686)$ decays [1], thus the uncertainty is about 0.6%.

The total systematic uncertainty is the sum in quadrature of all uncertainties added for each χ_{cJ} decay.

VI. SUMMARY

Using the $(448.1 \pm 2.9) \times 10^6$ $\psi(3686)$ events accumulated with the BESIII detector, the study of

$\chi_{cJ} \rightarrow \Sigma^+ \bar{p} K_S^0$ ($J = 0, 1, 2$) is performed for the first time, and clear χ_{cJ} signals are observed. The branching fractions of $\chi_{cJ} \rightarrow \Sigma^+ \bar{p} K_S^0$ are determined to be $(3.52 \pm 0.19 \pm 0.21) \times 10^{-4}$, $(1.53 \pm 0.10 \pm 0.08) \times 10^{-4}$, and $(8.25 \pm 0.83 \pm 0.49) \times 10^{-5}$ for $J = 0, 1$, and 2 , respectively, where the first and second uncertainty are the statistical and systematic ones, respectively. Due to the limited statistics, no evident structure is observed in the invariant mass of any subsystem.

ACKNOWLEDGMENTS

The BESIII collaboration thanks the staff of BEPCII and the IHEP computing center for their strong support. This work is supported in part by National Key Basic Research Program of China under Contract No. 2015CB856700; National Natural Science Foundation of China (NSFC) under Contracts Nos. 11625523, 11635010, 11735014, 11822506, 11835012; the Chinese Academy of Sciences (CAS) Large-Scale Scientific Facility Program; Joint Large-Scale Scientific Facility Funds of the NSFC and CAS under Contracts Nos. U1532257, U1532258, U1732263, U1832207; CAS Key Research Program of Frontier Sciences under Contracts Nos. QYZDJ-SSW-SLH003, QYZDJ-SSW-SLH040; 100 Talents Program of CAS; INPAC and Shanghai Key Laboratory for Particle Physics and Cosmology; ERC under Contract No. 758462; German Research Foundation DFG under Contracts Nos. Collaborative Research Center CRC 1044, FOR 2359; Istituto Nazionale di Fisica Nucleare, Italy; Ministry of Development of Turkey under Contract No. DPT2006K-120470; National Science and Technology fund; STFC (United Kingdom); The Knut and Alice Wallenberg Foundation (Sweden) under Contract No. 2016.0157; The Royal Society, UK under Contracts Nos. DH140054, DH160214; The Swedish Research Council; U. S. Department of Energy under Contracts Nos. DE-FG02-05ER41374, DE-SC-0010118, DE-SC-0012069; University of Groningen (RuG) and the Helmholtzzentrum fuer Schwerionenforschung GmbH (GSI), Darmstadt.

[1] M. Ablikim *et al.* (BESIII Collaboration), Chin. Phys. C **42**, 023001 (2018).

[2] M. Ablikim *et al.* (BESIII Collaboration), Nucl. Instrum. Methods Phys. Res., Sect. A **614**, 345 (2010).

Table II. Systematic uncertainty sources and their contributions (in %).

Source	$\mathcal{B}(\chi_{c0})$	$\mathcal{B}(\chi_{c1})$	$\mathcal{B}(\chi_{c2})$
Photon detection	3.0	3.0	3.0
PID and tracking	0.6	0.5	0.4
4C kinematic fit	0.4	0.4	0.3
K_S^0 reconstruction	1.2	1.2	1.2
π^0 mass window	0.3	0.3	0.3
K_S^0 mass window	0.3	0.3	0.3
Σ^+ mass window	0.1	0.1	0.1
Efficiency	1.0	0.9	0.4
Signal line shape	1.4	1.9	0.4
Mass and width of χ_{cJ}	3.0	0.4	3.9
Fit range	0.9	1.4	0.8
Background shape	2.8	1.4	1.5
Intermediate decay	2.1	2.6	2.2
Number of $\psi(3686)$	0.6	0.6	0.6
Total	6.0	5.2	5.9

- [3] M. Tanabashi *et al.* (Particle Data Group), Phys. Rev. D **98**, 030001 (2018).
- [4] S. Capstick and W. Roberts, Prog. Part. Nucl. Phys. **45**, S241 (2000).
- [5] M. Ablikim *et al.* (BESIII Collaboration), Phys. Rev. D **88**, 112001 (2013).
- [6] M. Ablikim *et al.* (BESIII Collaboration), Phys. Rev. D **87**, 032007 (2013).
- [7] M. Ablikim *et al.* (BESIII Collaboration), Phys. Rev. D **97**, 052011 (2018).
- [8] P. Naik *et al.* (CLEO Collaboration), Phys. Rev. D **78**, 031101 (2008).
- [9] C. H. Yu *et al.*, Proceedings of IPAC **2016** (2016).
- [10] S. Agostinelli *et al.* (GEANT4 Collaboration), Nucl. Instrum. Methods Phys. Res., Sect. A **506**, 250 (2003).
- [11] S. Jadach, B. F. L. Ward, and Z. Wąs, Comput. Phys. Commun. **130**, 260 (2000).
- [12] S. Jadach, B. F. L. Ward, and Z. Wąs, Phys. Rev. D **63**, 113009 (2001).
- [13] R. G. Ping, Chin. Phys. C **32**, 599 (2008).
- [14] D. J. Lange, Nucl. Instrum. Methods Phys. Res., Sect. A **462**, 152 (2001).
- [15] J. C. Chen, G. S. Huang, X. R. Qi, D. H. Zhang, and Y. S. Zhu, Phys. Rev. D **62**, 034003 (2000).
- [16] W. M. Tanenbaum *et al.*, Phys. Rev. D **17**, 1731 (1978).
- [17] G. R. Liao, R. G. Ping, and Y. X. Yang, Chin. Phys. Lett. **26**, 051101 (2009).
- [18] M. Xu *et al.*, Chin. Phys. C **33**, 428 (2009).
- [19] R. E. Mitchell *et al.* (CLEO Collaboration), Phys. Rev. Lett. **102**, 011801 (2009).
- [20] M. Ablikim *et al.* (BESIII Collaboration), Phys. Rev. D **92**, 052003 (2015).
- [21] M. Ablikim *et al.* (BESIII Collaboration), Phys. Rev. D **99**, 032006 (2019).
- [22] M. Ablikim *et al.* (BESIII Collaboration), Phys. Rev. D **87**, 012002 (2013).
- [23] M. Ablikim *et al.* (BESIII collaboration), Phys. Rev. D **92**, 112008 (2015).
- [24] M. Ablikim *et al.* (BESIII collaboration), Phys. Rev. D **95**, 072004 (2017).
- [25] V. V. Anashin *et al.* (KEDR Collaboration), Int. J. Mod. Phys. Conf. Ser. **02**, 188 (2011).